Three-dimensional coupled mode analysis of internal-wave acoustic ducts

Alexey A. Shmelev,[a] James F. Lynch,[b] and Ying-Tsong Lin
Applied Ocean Physics and Engineering Department, Woods Hole Oceanographic Institution, Woods Hole, Massachusetts 02543

Henrik Schmidt
Department of Mechanical Engineering, Massachusetts Institute of Technology, 77 Massachusetts Avenue, Cambridge, Massachusetts 02139

(Received 7 May 2013; revised 11 March 2014; accepted 18 March 2014)

A fully three-dimensional coupled mode approach is used in this paper to describe the physics of low frequency acoustic signals propagating through a train of internal waves at an arbitrary azimuth. A three layer model of the shallow water waveguide is employed for studying the properties of normal modes and their coupled interaction due to the presence of nonlinear internal waves. Using a robust wave number integration technique for Fourier transform computation and a direct global matrix approach, an accurate three-dimensional coupled mode full field solution is obtained for the tonal signal propagation through straight and parallel internal waves. This approach provides accurate results for arbitrary azimuth and includes the effects of backscattering. This enables one to provide an azimuthal analysis of acoustic propagation and separate the effects of mode coupled transparent resonance, horizontal reflection and refraction, the horizontal Lloyd's mirror, horizontal ducting and anti-ducting, and horizontal tunneling and secondary ducting.
 [http://dx.doi.org/10.1121/1.4869847]

PACS number(s): 43.20.Bi, 43.20.Mv, 43.30.Bp [KML] Pages: 2497–2512

I. INTRODUCTION

Internal waves are commonly observed in shallow waters and at continental shelf breaks. Over the last several decades, much effort has been expended on studying low-frequency acoustic propagation through shallow water internal waves. In the 1980s Yellow Sea experiments, Zhou *et al.*[1] showed and theoretically explained very strong (up to 25 dB) resonance-like intensity fluctuations that are both frequency and internal wave direction dependent. Preisig and Duda[2,3] studied the impact of individual soliton-type internal waves on normal mode coupling physics and clearly showed its dependence on wave width, amplitude and acoustic frequency. In the 1995 Shallow Water Acoustics in a Random Medium Experiment (SWARM95),[4] strong mode coupling was observed and studied statistically[5] for the across internal wave propagation direction. Also as part of the SWARM95 experiment, Badiey *et al.*[6] measured acoustic signals for an along waves path and showed that strong intensity fluctuations are caused by horizontal ducting of acoustic signals between internal waves. This was the first experimental evidence of an out of vertical plane acoustic interaction with internal waves, which was predicted theoretically[7] and numerically.[8,9] The Shallow Water 2006 Experiment (SW06[10]) was the first effort that concentrated on measuring the fully three-dimensional variability of the water column as well as acoustic signals coming from both the across and along internal waves directions. For that experiment, both intensity and horizontal angles of arrival fluctuations were observed[11,12] for the along internal wave acoustic track with a fixed source and receiving array.

The first experimental evidence of the horizontal Lloyd's mirror, an inherently three-dimensional acoustic effect, was observed in SW06 by Badiey *et al.*[13] Also as a part of the SW06, Lynch *et al.*[14] presented results on intensity fluctuations and their azimuthal dependence for a mobile source acoustic signal. In parallel to the experimental results, extensive analytical studies of the three-dimensional effects of internal wave natural curvature[15,16] and termination[17] on acoustic propagation were performed.

In this paper we will use a fully three-dimensional (3D) coupled mode approach to solve the problem of low-frequency acoustic propagation through straight and parallel internal waves for all azimuths. We will first study mode coupling at a vertical interface that divides the waveguide into two stratified half spaces: an unperturbed part and a perturbed part (for example, from the presence of nonlinear internal waves). Using this approach enables us to explicitly show the governing physics of mode coupled reflection from and transmission through internal waves. The precise 3D full field solution for internal waves with continuous waveforms will then be obtained using a 3D coupled mode program. This program is based on an algorithm that utilizes the independence of waveguide properties on one of the three spatial coordinates (along the internal wave crests) by means of a Fourier transform. Consequent application of the direct global matrix approach and wave number integration

[a]Current address: Schlumberger, Schlumberger House, Gatwick Airport, RH60NZ United Kingdom.
[b]Author to whom correspondence should be addressed. Electronic mail: jlynch@whoi.edu

provides accurate solutions for the 3D coupled mode acoustic field. A similar approach was used by Schmidt in his SAFARI propagation code[18] for range independent waveguides without mode coupling, and we extend it here to coupled mode propagation in an environment whose properties change in two dimensions.

Using the 3D coupled mode program, we study several 3D acoustic effects caused by a train of parallel internal waves, including coupled mode horizontal acoustic reflection from internal waves, the horizontal Lloyd's mirror (HLM), ducting and anti-ducting between internal waves, secondary ducting, coupled mode ducting, and coupled mode transparent resonance.

The composition of this paper is as follows. In Sec. II we will start with a brief overview of mode coupling theory and its simplification for waveguides whose properties change slowly in the horizontal. We then proceed with a fundamental problem: that of plane wave mode coupling at a vertical interface that divides two horizontally stratified waveguides. We provide the analytical solution for plane wave fronts and point sources in such an environment. In Sec. III, we introduce a simplified model of internal waves represented by combinations of vertical interfaces and study the physics of acoustic propagation for single internal waves. Multiple internal wave cases will be considered in Sec. IV. The precise 3D coupled mode numerical solution for single and multiple internal waves with smooth waveforms will be presented in Sec. V. Finally, the summary and future work directions will be discussed in Sec. VI.

II. THEORY

This section briefly covers the basics of acoustic mode coupling. In Sec. II A, we derive the general 3D coupled mode equation for range dependent waveguides and provide its simplified form for waveguides whose properties change slowly in the horizontal plane (adiabatic approximation). It will become clear later in this paper when such an approximation is appropriate in the presence of nonlinear internal waves. In Secs. II B and II C we consider the special case of mode coupling at a vertical interface that divides the waveguide into two stratified half planes, and obtain solutions for incident modes with plane wave and cylindrical wave fronts. This simplified problem will serve a basis for the 3D mode coupling for more sophisticated examples, shown in Secs. III and IV.

A. 3D coupled mode equation

Let us start with the Helmholtz equation for a point source in Cartesian coordinates,

$$\rho\frac{\partial}{\partial x}\left[\frac{1}{\rho}\frac{\partial p}{\partial x}\right]+\rho\frac{\partial}{\partial y}\left[\frac{1}{\rho}\frac{\partial p}{\partial y}\right]+\rho\frac{\partial}{\partial z}\left[\frac{1}{\rho}\frac{\partial p}{\partial z}\right]+\frac{\omega^2}{c^2(x,y,z)}p = -\delta(x-x_s)\delta(y-y_s)\delta(z-z_s), \quad (1)$$

where $c(x, y, z)$ is sound speed, $\rho(x, y, z)$ is density, $p(x, y, z)$ is acoustic pressure, and (x_s, y_s, z_s) is the source position. To solve for the sound pressure, we employ a vertical mode decomposition,

$$p(x,y,z)=\sum_m \Phi_m(x,y)\Psi_m(x,y,z), \quad (2)$$

where $\Phi_m(x, y)$ are the complex modal amplitudes and $\psi_m(x, y, z)$ are the normal modes at (x, y) obtained from the following equation:

$$\rho\frac{\partial}{\partial z}\left[\frac{1}{\rho}\frac{\partial\Psi_m(x,y,z)}{\partial z}\right]+\left[\frac{\omega^2}{c^2(x,y,z)}-k_{rm}^2(x,y)\right]\times\Psi_m(x,y,z)=0, \quad (3)$$

$k_{rm}(x,y)$ is the horizontal wave number of mode m, and appropriate boundary conditions will be imposed at the sea surface and the seabed. By substituting Eq. (2) into Eq. (1), and applying the operator

$$\int(\cdot)\frac{\Psi_n(x,y,z)}{\rho(z)}dz,$$

one can get

$$\frac{\partial^2\Phi_n}{\partial x^2}+\frac{\partial^2\Phi_n}{\partial y^2}+k_{rn}^2(x,y)\Phi_n+\sum_m A_{mn}\Phi_m+\sum_m B_{mn}\frac{\partial\Phi_m}{\partial x}+\sum_m C_{mn}\frac{\partial\Phi_m}{\partial y} = -\delta(x-x_s)\delta(y-y_s)\frac{\Psi_n(x,y,z_s)}{\rho(z_s)}, \quad (4)$$

where the mode coupling coefficients A_{mn}, B_{mn}, and C_{mn} are defined by

$$A_{mn}=\int\left(\rho\frac{\partial}{\partial x}\left[\frac{1}{\rho}\right]\frac{\partial\Psi_m}{\partial x}+\rho\frac{\partial}{\partial y}\left[\frac{1}{\rho}\right]\frac{\partial\Psi_m}{\partial y}\right)\frac{\Psi_n}{\rho}dz, \quad (5)$$

$$B_{mn}=\int\left(2\frac{\partial\Psi_m}{\partial x}+\rho\frac{\partial}{\partial x}\left[\frac{1}{\rho}\right]\Psi_m\right)\frac{\Psi_n}{\rho}dz, \quad (6)$$

and

$$C_{mn}=\int\left(2\frac{\partial\Psi_m}{\partial y}+\rho\frac{\partial}{\partial y}\left[\frac{1}{\rho}\right]\Psi_m\right)\frac{\Psi_n}{\rho}dz. \quad (7)$$

In general, the equations for the vertical and horizontal parts of the acoustic pressure are coupled, and for 3D varying environments, one has to solve the complete set of Eqs. (3)–(7). However, for environments whose parameters change in the horizontal slowly compared to the acoustic wavelength, the coupling coefficients are small, and the equations for modal amplitudes are approximated as

$$\frac{\partial^2\Phi_n}{\partial x^2}+\frac{\partial^2\Phi_n}{\partial y^2}+k_{rn}^2(x,y)\Phi_n = -\delta(x-x_s)\delta(y-y_s)\frac{\Psi_n(x,y,z_s)}{\rho(z_s)}. \quad (8)$$

Equation (8) is called the horizontal refraction equation[19] and the corresponding approximation is called the adiabatic

approximation. For acoustic propagation in the directions perpendicular to internal waves crests, the waveguide properties change rapidly, and this approximation is often not valid.[20] However, it will be shown by numerical simulations later in this paper that the adiabatic approximation is a reasonable approximation for shallow horizontal angles between the acoustic propagation track and the internal wave crests. In Secs. III and IV we will approach the full mode coupling problem for the simplified case of waveguides whose properties change in two spatial dimensions and are fixed in the third dimension.

B. Vertical interface: An incident mode with a plane wave front

Let us consider a vertical interface that divides a waveguide into two range independent half spaces 0 and 1 such that the waveguide in region 0 has the properties of an unperturbed waveguide and region 1 has slightly different water column properties. This scenario is an extreme case of rapidly changing properties in horizontal plane, and not realistic for many ocean features, since ocean properties generally change more gradually with horizontal distance. However, the basic physics of coupled mode reflection from and transmission through such an interface is similar to the real world internal wave scenario, and it also can be explained analytically, as will be shown below.

When studying the effects of mode coupling, it is a standard practice to consider the incident field due to each of the excited normal modes separately.[2,21] For now, we let the initial acoustic signal be a single mode n in the unperturbed region 0 with a horizontally plane wave front and unit amplitude at angular frequency ω. Figure 1 shows the top view of the medium. We define axis x along the vertical interface and axis y perpendicular to the interface with positive direction pointing towards region 0. Vertical axis z with zero value at the ocean surface has positive direction into the seabed.

The horizontally stratified region 0 is associated with the set of unperturbed modes Ψ_n^0 and horizontal modal wave numbers k_{rn}^0. Region 1 is also horizontally stratified, but its waveguide properties are slightly different from region 0. It is characterized by a perturbed set of modes Ψ_n^1 and horizontal modal wave numbers k_{rn}^1.

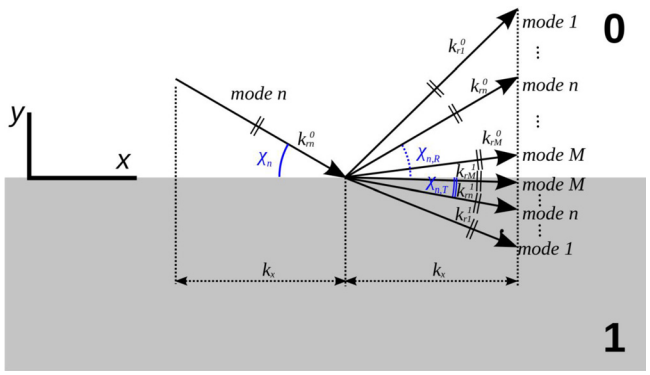

FIG. 1. (Color online) Top view of plane wave mode coupling at a vertical interface. The incident pressure field consists of a single mode n of unit amplitude with grazing angle χ_n. Along the interface, it couples into all propagating modes $1, \ldots, M$ of both the reflected and transmitted fields.

Define the horizontal grazing angle χ_n as the angle between horizontal wave vector of incident mode n and the x axis as shown in Fig. 1. The incident pressure field then can be written as

$$p_I = \Psi_n^0(z) e^{ik_{rn}^0 (x\cos\chi_n - y\sin\chi_n)}. \tag{9}$$

In order to ensure the continuity of the acoustic pressure and the normal component of particle velocity at the vertical interface, we set

$$p_I(x, y=0, z) + p_R(x, y=0, z) = p_T(x, y=0, z),$$
$$\frac{1}{\rho^0(z)}\left(\frac{\partial p_I}{\partial y}\bigg|_{y=0} + \frac{\partial p_R}{\partial y}\bigg|_{y=0}\right) = \frac{1}{\rho^1(z)}\frac{\partial p_T}{\partial y}\bigg|_{y=0}, \tag{10}$$

where $\rho^0(z)$ and $\rho^1(z)$ are the vertical density functions in the regions 0 and 1, respectively. In this work density changes due to the ocean thermocline depression are considered weak compared to the water-seabed density contrast, and therefore $\rho^0(z) \approx \rho^1(z) \approx \rho(z)$. One must also allow the reflected and transmitted fields, p_R and p_T, to comprise all the propagating modes, i.e.,

$$p_R = \sum_{m=1}^{M} R_{nm}(\chi_n)\Psi_m^0(z) e^{ik_{rm}^0 (x\cos\chi_{m,R} + y\sin\chi_{m,R})},$$
$$p_T = \sum_{m=1}^{M} T_{nm}(\chi_n)\Psi_m^1(z) e^{ik_{rm}^1 (x\cos\chi_{m,T} - y\sin\chi_{m,T})}, \tag{11}$$

where R_{nm} and T_{nm} are the coefficients of the plane wave mode coupled reflection and transmission of incident mode n into mode m, $\chi_{m,R}$, and $\chi_{m,T}$ are the horizontal grazing angles of coupled mode m in the reflected and transmitted fields, respectively (Fig. 1), and M is the number of propagating modes. Equation (11) is missing the continuous part of the wavenumber spectrum. At a vertical sharp interface, mode coupling will result in energy leakage into the continuous part of the spectrum. In the current study we neglect this part of acoustic energy. We note, however, that there are several available algorithms that account for the continuous spectrum. One of them[22] uses the "leaky modes" approximation and could potentially be useful. The "leaky modes" have exponentially increasing amplitude in the fluid half space, and the fact that they are not perfectly orthogonal to the trapped modes complicates the analysis. We therefore leave this for further research study and only consider the discrete part of the spectrum. As a result, the solutions obtained in the current paper have a vertical angle limitation.

The boundary conditions given by Eq. (10) provide the continuity of the x-component of horizontal wave number (Snell's law) for both reflected and transmitted modes,

$$k_x \equiv k_{rn}^0 \cos\chi_n = k_{rm}^0 \cos\chi_{m,R} = k_{rm}^1 \cos\chi_{m,T},$$
$$m = 1, \ldots, M. \tag{12}$$

They also provide linear relations for the coupled reflection and transmission coefficients,

$$\delta_{nm} + R_{nm}(\chi_n) = \sum_{k=1}^{M} T_{nk}(\chi_n) \times \int \frac{\Psi_k^1(z)\Psi_m^0(z)}{\rho(z)} dz, \quad m = 1, \ldots, M,$$
$$\delta_{nm}\tan\chi_n + R_{nm}(\chi_n)\tan\chi_{m,R} = \sum_{k=1}^{M} T_{nk}(\chi_n)\tan\chi_{k,T} \int \frac{\Psi_k^1(z)\Psi_m^0(z)}{\rho(z)} dz, \quad m = 1, \ldots, M, \tag{13}$$

where δ_{nm} is the Kronecker symbol. The values of the mode coupled reflection and transmission coefficients $R_{nm}(\chi_n)$ and $T_{nm}(\chi_n)$ are obtained by solving the set of linear equations (13) for each incident mode number n and specified grazing angle χ_n.

C. Vertical interface: Point source solution

Having solved the mode coupling problem at the vertical interface for a single incident mode with a plane wave front, it is possible to obtain the solution for the acoustic pressure field on both sides of the vertical interface due to a point source located in region 0 at (x_s, y_s, z_s). Since the waveguide is independent of the x-coordinate, we set $x_s = 0$ for convenience. By applying the one-dimensional Fourier transform (FT) operator,

$$\mathrm{FT}\{\cdot\} = \frac{1}{2\pi}\int_{-\infty}^{+\infty} \{\cdot\} e^{-ik_x x} dx, \tag{14}$$

to both sides of Eq. (1), and assuming no density variation in the horizontal, we get a two-dimensional separable Helmholtz equation

$$\frac{\partial^2 \tilde{p}(k_x, y, z)}{\partial y^2} + \frac{\partial^2 \tilde{p}(k_x, y, z)}{\partial z^2} + \left[\frac{\omega^2}{c^2(y,z)} - k_x^2\right]\tilde{p}(k_x, y, z) = -\frac{\delta(y - y_s)\delta(z - z_s)}{2\pi}. \tag{15}$$

As before, we start with considering the portion of the acoustic energy due to the excitation of a single mode. The solution of Eq. (15) for an excited mode n can be formally written as

$$\tilde{p}_n(k_x, y, z) = \begin{cases} \sum_{m=1}^{M}\left[\Phi_{nm}^{(0)+} e^{ik_{ym}^0(k_x)y} + \Phi_{nm}^{(0)-} e^{-ik_{ym}^0(k_x)y}\right]\Psi_m^0(z) + \tilde{p}_n^s(k_x, y, z), & y \geq 0, \\ \sum_{m=1}^{M}\left[\Phi_{nm}^{(1)+} e^{ik_{ym}^1(k_x)y} + \Phi_{nm}^{(1)-} e^{-ik_{ym}^1(k_x)y}\right]\Psi_m^1(z), & y < 0. \end{cases} \tag{16}$$

In the above the single mode free-field source term $\tilde{p}_n^s(k_x, y, z)$ is the solution of Eq. (1) for the range independent waveguide,[19]

$$\tilde{p}_n^s(k_x, y, z) = \frac{i}{4\pi\rho(z_s)}\Psi_n^0(z_s)\Psi_n^0(z)\frac{e^{ik_{yn}^0(k_x)|y - y_s|}}{k_{yn}^0(k_x)}, \tag{17}$$

where $k_{ym}^0(k_x)$ and $k_{ym}^1(k_x)$ are the y-components of the horizontal wave number of mode m in regions 0 and 1, respectively,

$$k_{ym}^j(k_x) = \begin{cases} \sqrt{(k_{rm}^j)^2 - k_x^2}, & k_x^2 \leq (k_{rm}^j)^2, \quad j = 0, 1, \\ i\sqrt{k_x^2 - (k_{rm}^j)^2}, & k_x^2 > (k_{rm}^j)^2, \quad j = 0, 1, \end{cases} \tag{18}$$

$\Phi_{nm}^{(0)+}$ and $\Phi_{nm}^{(0)-}$ are the amplitudes of mode m coupled from incident mode n and traveling in the positive and negative directions of y axis, respectively, in region 0, and $\Phi_{nm}^{(1)+}$ and $\Phi_{nm}^{(1)-}$ are similar amplitudes in the perturbed region 1. The Sommerfeld radiation condition requires that

$$\Phi_{nm}^{(0)-} = 0, \quad m = 1, \ldots, M,$$
$$\Phi_{nm}^{(1)+} = 0, \quad m = 1, \ldots, M. \tag{19}$$

Equation (17) for $y < y_s$ describes the incident field that consists of a single mode n with a plane wave front. Following the procedure shown in Sec. II B we can derive the other two coefficients in Eq. (16),

$$\Phi_{nm}^{(0)+}(k_x) = \frac{i}{4\pi\rho(z_s)}\frac{\Psi_n^0(z_s)e^{ik_{yn}^0 y_s}}{k_{yn}^0}R_{nm}(\chi_n),$$
$$\Phi_{nm}^{(1)-}(k_x) = \frac{i}{4\pi\rho(z_s)}\frac{\Psi_n^0(z_s)e^{ik_{yn}^0 y_s}}{k_{yn}^0}T_{nm}(\chi_n), \tag{20}$$

where the horizontal grazing angle χ_n is related to the components of the modal wave number by

$$\chi_n = \cos^{-1}\frac{k_x}{k_{rn}^0}. \tag{21}$$

Acoustic pressure as a function of x is obtained by applying the one-dimensional inverse Fourier transform (IFT) operator

$$\mathrm{IFT}\{\cdot\} = \int_{-\infty}^{+\infty} \{\cdot\} e^{ik_x x} dk_x, \tag{22}$$

to both sides of Eq. (16). Using Eq. (19), Eq. (20), and the method of stationary phase, the Fourier integral can be evaluated for each coupled mode m at its stationary points $k_x^s(n,m)$. As a result, the acoustic pressure due to mode n excited at the source location approximates to

$$p_n(x,y,z) \approx \begin{cases} \dfrac{\Psi_n^0(z_s)e^{i\pi/4}}{\sqrt{8\pi}\rho(z_s)}\Psi_m^0(z)\dfrac{e^{ik_{rn}^0}}{\sqrt{k_{rn}^0 r}} + \dfrac{\Psi_n^0(z_s)e^{i\pi/4}}{\sqrt{8\pi}\rho(z_s)}\displaystyle\sum_{m=1}^{M} R_{nm}(\chi_n^s)\Psi_m^0(z)\dfrac{\exp i(k_{rn}^0 r_1 + k_{rm}^0 r_2)}{\left(k_{rn}^0 r_1 + \left(\dfrac{k_{yn}^0}{k_{ym}^0}\right)^2 k_{rm}^0 r_2\right)^{1/2}}, & y \geq 0, \\ \dfrac{\Psi_n^0(z_s)e^{i\pi/4}}{\sqrt{8\pi}\rho(z_s)}\displaystyle\sum_{m=1}^{M} T_{nm}(\chi_n^s)\Psi_m^1(z)\dfrac{\exp i(k_{rn}^0 r_1 + k_{rm}^1 r_2)}{\left(k_{rn}^0 r_1 + \left(\dfrac{k_{yn}^0}{k_{ym}^1}\right)^2 k_{rm}^1 r_2\right)^{1/2}}, & y < 0. \end{cases} \tag{23}$$

In the expression above,

$$\chi_n^s(m) = \cos^{-1}\frac{k_x^s(n,m)}{k_{rn}^0} \tag{24}$$

and

$$\chi_m^{s,\text{coupled}}(n) = \begin{cases} \cos^{-1}\dfrac{k_x^s(n,m)}{k_{rm}^0}, & y \geq 0, \\ \cos^{-1}\dfrac{k_x^s(n,m)}{k_{rm}^1}, & y < 0 \end{cases} \tag{25}$$

are the horizontal grazing angles of initial mode n and reflected (or transmitted) coupled mode m, respectively, for the stationary point $k_x^s(n, m)$ (Fig. 2), r is the horizontal distance between the source and the receiver, and $r_1(n,m)$ and $r_2(n,m)$ are the lengths of the two-segmented refracted eigenrays connecting the source and the receiver such that

$$r_1 = \frac{y_s}{\sin\chi_n^s(m)}, \quad r_2 = \frac{|y|}{\sin\chi_m^{s,\text{coupled}}(n)}. \tag{26}$$

Note that for $m = n$, $\chi_n^s(m) = \chi_m^{s,\text{coupled}}(m)$, which implies the specular reflection of initial mode n. Equation (23) approximates the portion of the acoustic pressure due to an individual mode n excited by the point source. The total acoustic pressure field for a point source is the sum of its components due to each excited mode

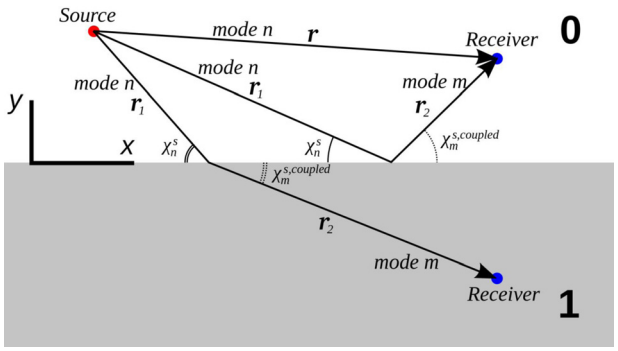

FIG. 2. (Color online) Geometrical approximation to the coupled mode horizontal reflection from and transmission through a vertical interface.

$$p(x,y,z) = \sum_{n=1}^{M} p_n(x,y,z). \tag{27}$$

Equations (23) and (27) represent a geometrical acoustic approximation to coupled mode propagation in the horizontal plane. Once the eigenray for the mode pair (n,m) is found from Eqs. (24)–(26), the acoustic pressure is easily computed. Figure 2 schematically illustrates the geometric approximation of mode coupled reflection and transmission at the vertical interface. The acoustic source is located in the region 0, and two possible locations of the receiver are shown in regions 0 and 1. For the receiver located in region 0, the solution due to initial mode n is a sum of the direct path contribution and the weighted sum of coupled modes traveling along the two-legged reflected eigenrays. For the receiver located in region 1, solution due to initial mode n is a weighted sum of the coupled modes traveling along the two-legged transmitted eigenrays. McMahon[23] obtained a similar to Eq. (23) result for an adiabatic approximation. Equations (23) and (27) provide the full 3D coupled mode point source solution.

III. SINGLE INTERNAL WAVE

Next, we will discuss the physics of acoustic normal mode propagation through a single internal wave at different horizontal grazing angles. To do this, we will use the waveguide model shown in Fig. 3. This is an idealized model that consists of two horizontal fluid layers bounded by a vacuum on the top and by the homogeneous fluid seabed below. The lower acoustic layer is characterized by a constant reference

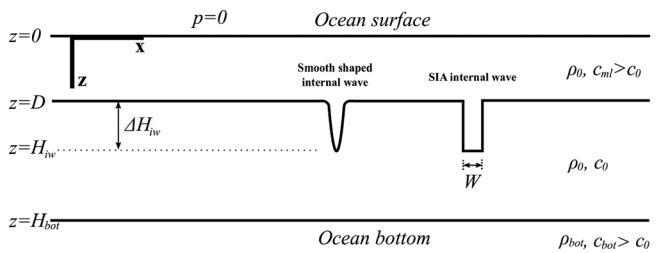

FIG. 3. Two waveguide model consists of two water layers (with upper layer having slightly faster sound speed than lower layer) overlaying ocean bottom, which is represented by fluid half space. Modeled smooth shaped internal wave is shown on the left, and its approximation by a sharp interface internal wave (SIA wave) is shown on the right.

sound speed c_0 and water density ρ_0. The upper layer, that is often called the mixed layer, has the same density, but a sound speed slightly higher than the reference sound speed, $c_{ml} = c_0 + \Delta c$. The homogeneous bottom has a constant density and sound speed equal to the seabed reference values c_{bot} and ρ_{bot}. The depth of the interface between layers is D and the a bottom depth is H_{bot}.

The waveguide model above does not fully accurately describe the vertical variation of sound speed, but it is fairly simple and at the same time approximates a wide range of shallow water columns, especially in the mid-latitude summer time or at low latitudes, when a higher sound speed surface mixed layer exists. Another advantage of this "canonical" waveguide is that internal waves are easily incorporated by lowering the horizontal interface between the water layers (see the left wave shape in Fig. 3).

In the previous section, we showed that a waveguide with a single vertical interface provides a useful solution that describes the geometric acoustics approximation for coupled mode horizontal propagation. We will use this approach again in this and the next sections and replace the smooth shaped internal wave by its top hat like approximation (see the right wave shape in Fig. 3). This approximation, which is also called the sharp interface approximation (SIA), models internal wave with two parallel vertical interfaces separated by offset W, such that the interface between water layers (thermocline) has the depth D everywhere outside such wave and is depressed to a new depth $H_{iw} = D + \Delta H_{iw}$ in between vertical interfaces (inside the internal wave).

The SIA internal wave is not a new approach, and was used by Preisig and Duda[2,3] to study 2D mode coupling effects and by Lin *et al.*[17] to study acoustic mode horizontal ducting between internal waves and radiation from an open duct under the adiabatic approximation. In this paper we use the SIA internal wave model to understand the fundamental physics of acoustic normal mode 3D propagation through internal waves, and not for numerical computations or quantitative studies. The advantage of the SIA wave is that it is simple and that the coupled mode reflection and transmission occurs only at two vertical interfaces, as opposed to continuous mode coupling inside smoother shaped internal waves. We will see that this simple model is capable enough to describe complicated 3D coupled mode effects that occur within real internal waves. In Sec. V we will also present numerical modeling results for smoothed shape internal waves, and see how the simple SIA and more realistic waveform calculations compare.

The front and back interfaces of SIA waves are sharp for any grazing angle, and at shallow grazing angles, the mode coupling strength in this model will be stronger than for the case of smooth shaped internal waves. To overcome this limitation, we will employ a hybrid approach of using the SIA internal waves and dividing the 3D propagation into three propagation direction sectors (similar to Badiey *et al.*[20]): steep, intermediate, and shallow horizontal grazing angles. With real internal waves, the water column sound speed changes quickly along the acoustic track at steep grazing angles. Mode coupling is strong and horizontal refraction is weak at these angles. On the other hand, for shallow horizontal grazing angles, propagation occurs in directions close to parallel to the internal wave crests, and the waveguide properties change slowly. Therefore, mode coupling is weak, and we can assume nearly adiabatic propagation with strong horizontal refraction at these angles. In the transition regime (intermediate grazing angles), both mode coupling and horizontal refraction are important and should be considered. The boundaries of these azimuthal sectors are not exact and depend on the amplitude of the internal wave. For the examples shown in numerical simulation in Sec. V, we consider the grazing angle to be shallow if it is equal or less than the maximum horizontal critical angle of the normal modes, which will be defined later in this section (typically less than ten degrees); intermediate grazing angles are approximately 10° to 35°; steep grazing angles are greater than 35°.

Addition of a second vertical interface provides another vertical discontinuity, and mode coupling becomes more complicated. We wish to understand how the finite width of the SIA wave alters the reflected and transmitted mode amplitudes as compared to the single sharp interface studied above. As before, a single mode incident with a cylindrical wave front is considered.

A. Transparent resonance and coupled cancellation

Let us start with steep grazing angles. Coupled mode propagation in directions perpendicular to the SIA internal wave crest directions (i.e., at a horizontal grazing angle of ninety degrees) was studied in detail by Duda and Preisig[2,3] among others. We will discuss two effects of the coupling physics from their study: transparent resonance and coupled cancellation. Consider an incident mode n coupled into mode m at the front interface of a SIA wave (top panel in Fig. 4). In the transparent resonance regime, the wave width is such that

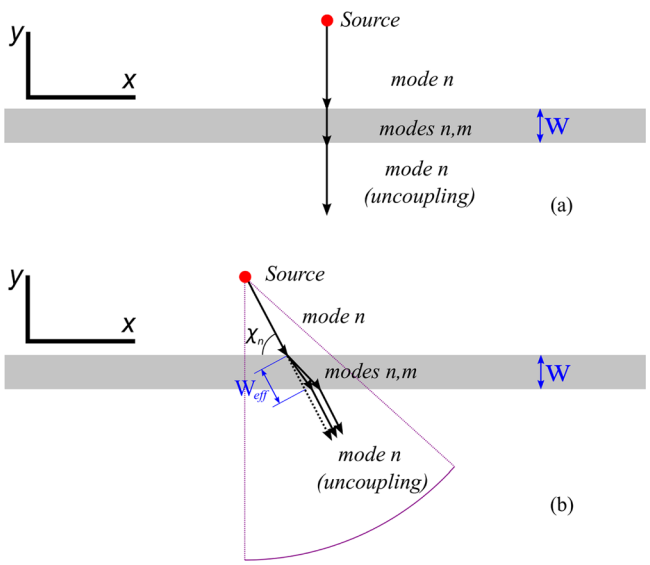

FIG. 4. (Color online) (a) Mode coupling diagram for normal incidence of mode n upon a SIA wave. Mode n partially couples into mode m at the front interface. At a certain resonant width of the wave, mode m uncouples back into mode n at the back interface. (b) Same scenario, but for steep (other than normal) grazing angle of initial mode n. Weak refraction of the coupled modes at these angles makes both segmented rays coincide with each other and with a straight (dashed) line.

the phase difference between modes n and m changes by an integer multiple of 2π as they travel across the wave[2,3]

$$W^{\text{res}} \approx \frac{2\pi l}{|k_{rn}^1 - k_{rm}^1|}, \quad l = 1, 2, \ldots . \tag{28}$$

The cancellation regime is a special case of transparent resonance, where the wave width W is short enough so that the relative phase difference between modes n and m does not change significantly as they reach the back interface of the wave, and "uncoupling" occurs (or put another way, "reverse coupling" occurs).

When the resonance condition is satisfied, energy of mode n coupled into mode m at the front sharp interface uncouples back into mode n at the back interface. Since only few significant (sometimes also called dominant) modes[2] carry most of the coupled energy within the SIA waves (and smooth-shaped waves), uncoupling of mode m back into mode n will result in almost total uncoupling of mode m if either of modes n or m is dominant.

For steep grazing angles, other than normal, it was shown[12] for internal waves with amplitudes of 5–40 m, acoustic frequencies of 50–500 Hz and the waveguide model used in the present work, that horizontal refraction of coupled modal rays is not significant for initial mode grazing angles greater than 35°–40°. Using the principles of the geometric approximation to mode coupling discussed in Sec. II and neglecting the effects of horizontal refraction, normal mode propagation through a SIA wave at steep grazing angles can be interpreted as follows: the horizontal ray of mode n coupled into mode m inside the wave coincides with the horizontal ray of mode n propagating through the wave [Fig. 4(b)] and both of them lay on an almost straight line. Therefore, the cancellation regime between initial mode n with grazing angle χ_n and mode m happens when the projection of the wave width onto the ray direction (effective wave width W_{eff}) satisfies the resonance condition

$$W^{\text{res,eff}} \equiv \frac{W}{\sin\chi_n} \approx \frac{2\pi l}{|k_{rm}^1 - k_{rn}^1|}, \quad l = 1, 2, \ldots . \tag{29}$$

Both the cancellation regime and the transparent resonance regime play important roles in the intensity fluctuations of the acoustic energy transmitted through an internal wave or a train of internal waves. If one measures modal amplitudes behind a wave along a circle arc centered at the source position [Fig. 4(b)], significant fluctuations are expected as the effective wave width passes through its resonant values.

B. Horizontal Lloyd's mirror

At shallow grazing angles (typically below 10° in the examples presented in this paper), horizontal refraction is important, and mode coupling is weak. Therefore, in this propagation regime, we will neglect mode coupling and assume single mode adiabatic reflection and refraction at the SIA wave interfaces. In Sec. II we studied the coupled mode reflection and transmission through a single vertical interface. For a source and a receiver located at one side of the vertical interface, Eq. (23) shows that the total solution should be direct path plus all coupled and non-coupled specular mode reflections. For incident grazing angles less than

$$\chi_{n,\text{crit}} = \cos^{-1}\frac{k_{rn}^1}{k_{rn}^0}, \tag{30}$$

the y component of the horizontal wave number of mode n in the perturbed region becomes imaginary, and under the adiabatic approximation below these angles total horizontal reflection of mode n occurs, i.e., $R_{nn} \approx 1$ for these angles. Horizontal grazing angles defined by Eq. (30) are called the critical grazing angle of mode n. The superposition of the direct arrival of mode n and its reflected part with subcritical grazing angles creates a strong interference pattern on the source side of internal wave that is called the horizontal Lloyd's mirror[24] (HLM). The classical Lloyd's mirror effect[25,26] is a dipole-like interference of a direct path and a path reflected from the sea surface in the vertical r-z plane. The HLM pattern differs from the classical Lloyd's mirror in that it happens in the horizontal plane and that reflection from the wave interface is only important at the subcritical grazing angles defined by Eq. (30). In the classical Lloyd's mirror, reflection from the sea surface is considered perfect at all vertical grazing angles. Another difference is the cylindrical spreading in the HLM, as opposed to spherical spreading in the classical Lloyd's mirror. Work by McMahon[23] provides theoretical studies of the HLM for straight and curved nonlinear internal wave fronts under the adiabatic approximation. The HLM effect has been observed experimentally in the Shallow Water 2006 experiment.[13]

The difference between the HLM effect at the single vertical interface, which is equivalent to an infinitely wide SIA internal wave, and a finite width SIA wave is due to the horizontal tunneling of normal modes. This effect allows partial energy leakage through the wave even at subcritical grazing angles. The resultant intensity of the reflected initial mode is expected to be slightly weaker. Below we explain the physics of this effect.

C. Horizontal tunneling through internal waves

Let us now return to the horizontal refraction equation [Eq. (8)] and apply the one-dimensional FT operator [Eq. (14)] to its homogeneous part,

$$\frac{\partial^2\Phi_n(y,k_x)}{\partial y^2} + (k_{rn}^2(y) - k_x^2)\Phi_n(y,k_x) = 0. \tag{31}$$

The modal horizontal wave number in the presence of a single SIA wave of width W is

$$k_{rn}(y) = \begin{cases} k_{rn}^0, & y < 0, \\ k_{rn}^1, & 0 \le y \le W, \\ k_{rn}^0, & y > W. \end{cases}$$

As before, we consider an initial acoustic field consisting of a single mode n with unit amplitude and a planar wave front, but incident upon the SIA wave of finite width W at a

subcritical grazing angle $\chi_n < \chi_{\mathrm{crit},n}$, and with no mode coupling. Since $k_{rn}^0 > k_x > k_{rn}^1$ at subcritical grazing angles, Eq. (31) represents a standard problem of particle transmission through a potential barrier in quantum mechanics.[27,28] The corresponding plane wave transmission coefficient is

$$T_n \approx \exp\left[-\int_0^W \sqrt{(k_x)^2 - (k_{rn}(y))^2}\,dy\right], \tag{32}$$

which for the SIA wave of width W is

$$T_n \approx \exp\left[-W\sqrt{(k_x)^2 - (k_{rn}^1)^2}\right]. \tag{33}$$

One can see that the transmission coefficient above is unity at the critical angle, and it rapidly decreases as the grazing angle becomes less than critical. Therefore, at subcritical grazing angles acoustic energy propagates through the wave, and the angular spectrum of the transmitted modal amplitude is localized in a narrow angular range just below its critical value. This effect is called horizontal tunneling. In ocean acoustics, tunneling in the vertical plane was observed numerically by Jensen and Schmidt[29] when studying Gaussian beam penetration through a sediment layer at subcritical vertical grazing angles. Horizontal tunneling through internal waves has recently been decomposed into the horizontal leaky modes of the horizontal ducts by Lin *et al.*[17] Energy leakage is an inherent property of the acoustic tunneling. As a result, reflection from the wave becomes imperfect at subcritical grazing angles under the adiabatic approximation.

D. Coupled mode reflections from internal waves

We discussed above that the subcritical grazing angles of normal modes are considered as shallow grazing angles, and for the numerical examples to be presented in Sec. V, mode coupling is indeed weak below approximately 10°. Consider now the 3D coupled mode effects in the transition sector between the steep and shallow grazing angles. Horizontal refraction of normal modes in our examples (Sec. V) is shown to be considerable for grazing angles up to approximately 35°. Thorough analysis of the coupled mode reflection coefficient (see Ref. 12 for details) shows that in the transition grazing angle sector (10°–35°), the coupled mode reflection coefficient R_{nm} for a single vertical interface as defined by Eq. (13) has peak values for certain mode pairs (n, m) and grazing angles of the incident mode n equal to

$$\chi_n \approx \cos^{-1}\frac{k_{rm}^1}{k_{rn}^0}. \tag{34}$$

Such features of the coupled reflection coefficient correspond to narrow beams of coupled mode energy reflected by the vertical interface (coupled mode reflection). Below this angle, coupled mode m is evanescent inside the internal wave. Therefore, when a finite width SIA wave is considered instead of a single vertical interface, the effect of horizontal tunneling may also alter the strength of this effect.

With realistically smooth wave shapes, mode coupling is continuous across the wave. When an initial mode n with a grazing angle above its critical value couples into mode m, whose grazing angle becomes subcritical, the resulting energy of mode m is available for horizontal tunneling. Therefore, although we discussed them separately, mode coupling and horizontal tunneling are interconnected effects.

IV. MULTIPLE INTERNAL WAVES

In real ocean environments, nonlinear internal waves usually travel in trains of several waves. Many acoustic and oceanographic experiments[1,4,10] provide evidence of strong time varying intensity fluctuations as a package of internal waves propagates in the vicinity of a source-to-receiver track. Therefore, it is important to understand what 3D acoustic effects one should expect as the train approaches and crosses the acoustic track at different angles. Below, we first describe one of the major causes of intensity fluctuations in the along-wave propagation scenario: acoustic ducting and anti-ducting.

A. Horizontal acoustic ducting

The horizontal reflection of acoustic normal modes from internal wave interfaces at subcritical angles was shown to cause significant contrasts in acoustic intensity compared to the "no wave present" case.[24] Therefore, as an internal wave train propagates through the source location, one would expect intensity fluctuations in the "near-crest" directions. The effect of horizontal acoustic ducting may be observed if an acoustic source is located between neighboring internal waves of depression. For such a scenario, a part of the mode n energy is confined within the grazing angle range $\lfloor -\chi_{n,\mathrm{crit}}, +\chi_{n,\mathrm{crit}} \rfloor$, i.e., is horizontally trapped by these waves due to almost total reflection at the subcritical grazing angles. Alternatively, if one puts an acoustic source inside an internal wave of depression, the horizontal ray of mode n with negligibly small initial grazing angle is pushed out from the wave with grazing angle $\pm\chi_{n,\mathrm{crit}}$. This effect is known as anti-ducting.[7]

Ducting of acoustic energy between waves implies no cylindrical spreading compared to the usual range independent environment. Contrariwise, anti-ducting has spreading stronger than cylindrical. Acoustic ducting contributes to longer propagation in the "along-crest" direction compared to the "no waves" background scenario. The combination of ducting and anti-ducting events creates very large scintillations of the acoustic intensity. These effects were first described for internal waves theoretically by Katsnelson and Pereselkov[7] and numerically by Badiey *et al.*[6] The first experimental observations of these strong intensity fluctuations (6–10 dB) compared to the "no waves" case, with an along wave geometry for internal waves passing over a fixed source and receiver, were made during the SWARM95 experiment.[6] Later, the SW06 experiment[10] was specifically configured for measuring three-dimensional acoustic effects,

and the intensity fluctuations in these directions were commonly observed in presence of internal wave trains.

B. Secondary tunneled ducting of normal modes

We showed that if mode coupling is not important, the effect of horizontal tunneling provides energy leakage through the internal waves even at subcritical grazing angles. When the tunneled acoustic signal encounters another wave in the train, part of its energy is reflected, and another part is tunneled further in the same manner as it did through the first wave. Ducted energy continues leaking at each consequent interaction with the waves (Fig. 5).

With the adiabatic tunneled transmission coefficient given in Eq. (33), and the conservation relation between reflection and transmission coefficients,

$$|R_n|^2 + |T_n|^2 = 1, \tag{35}$$

the amplitude of mode n in the secondary duct after l interactions with the waves is proportional to

$$|\Phi_n| \approx T_n R_n^l \approx e^{-W\sqrt{(k_x)^2-(k_{rn}^1)^2}}\left(1 - e^{-W\sqrt{(k_x)^2-(k_{rn}^1)^2}}\right)^{l/2}. \tag{36}$$

The leakage rate associated with tunneling is high at grazing angles that are close to the critical values. On the other hand, the reflection coefficient is greater further below the critical grazing angles (since the exponent in the second brackets quickly vanishes as k_x exceeds k_{rn}^1). Therefore, the angular spectrum of the acoustic field in the secondary duct narrows as l increases.

V. NUMERICAL MODELING

In this section, we will evaluate the three-dimensional effects of acoustic propagation in the presence of parallel internal waves that have a smooth shape that is closer to the natural shapes observed. Although this scenario also is not realistic for the ocean, as perfectly straight internal waves never exist, the following numerical examples demonstrate the quantitative importance of the fundamental mechanisms discussed in previous sections, specifically the horizontal modal refraction and normal mode coupling, which govern acoustic propagation through real ocean waveguides.

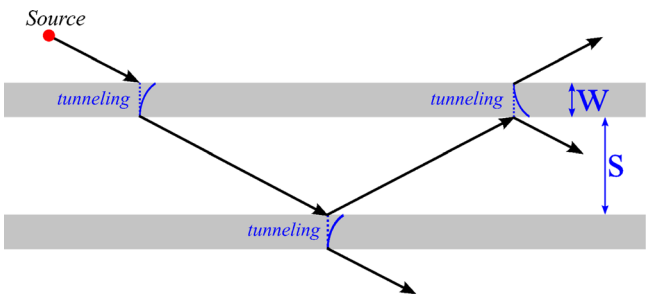

FIG. 5. (Color online) Secondary ducting due to mode tunneling. Partially ducted energy leaks out from the duct during each interaction with the waves.

Numerical methods for three-dimensional acoustics coupled mode propagation in range dependent environments are complicated and generally require a considerable amount of computing power and memory. Three-dimensional PE techniques[30,31] are perhaps the most efficient ways to accomplish the task of creating a pressure field numerically. In parallel internal waves applications, we can eliminate the dependence in the direction along the wave crests. For such cases, there exists a useful Fourier transform based method[32,33] that allows one to divide a three-dimensional mode coupling problem into many standard[34] two-dimensional problems (see Appendix A for details). This technique is useful for mode calculations, since it gives the precise solution and allows all grazing angles as well as backscattering to be taken into account, unlike other available PE algorithms.

The two-layer background waveguide model, which was discussed in previous sections, will be used for our simulations with the following parameters: $c_0 = 1500$ m/s, $c_{ml} = 1530$ m/s, $c_{\text{bot}} = 1800$ m/s, $\rho_0 = 1000$ kg/m^3, $H = 80$ m, and $D = 15$ m. We model internal waves by displacing the interface between the water layers, but for modeling more realistic scenarios we use the smooth wave shape this time (left wave in Fig. 3). A sech^2 function is used for modeling the shape of internal waves (solitons),

$$H_{iw}(y) = D + \Delta H_{iw}\,\text{sech}^2\left(\frac{y - y_{\text{wave}}}{W}\right), \tag{37}$$

where $\Delta H_{iw} = 25$ m is the amplitude of the wave used in the simulations, $W = 70$ m is the width parameter, and y_{wave} is the coordinate of the wave center. Such a wave shape is as a formal solution to the Korteweg–de Vries equation[35] describing the propagation of weakly nonlinear internal waves. The half-amplitude width of this wave is 130 m. Figure 6(a) shows the shape of this wave (black line). In our numerical modeling, one hundred steps are used to divide the waveguide inside the wave into locally range independent sectors (the blue line in the upper panel of Fig. 6). The source frequency is considered to be 100 Hz. The KRAKEN normal mode code[36] was used for computation of mode functions and horizontal wave numbers across the wave.

Corrections to the horizontal wave numbers of the normal modes for the sectors inside the wave, with respect to background water column values, are shown in Fig. 6(b). The lower panel of the same figure shows the horizontal critical angles of the normal modes, which were computed with Eq. (30). Note the minimum and maximum horizontal critical angles of 5° and 8°, respectively.

A. Single wave

We start our modeling with a single internal wave centered along $y_{\text{wave}} = 0$ m and an acoustic source at $x_s = 0$ m, $y_s = 500$ m. For visualizing the effects of mode coupling, we let the incident field consist of a single mode with unit amplitude at 1 m distance from the source. Figure 7 shows amplitudes of modes 1–4 for the case of incident mode 1. The crest of the internal wave is schematically shown by the

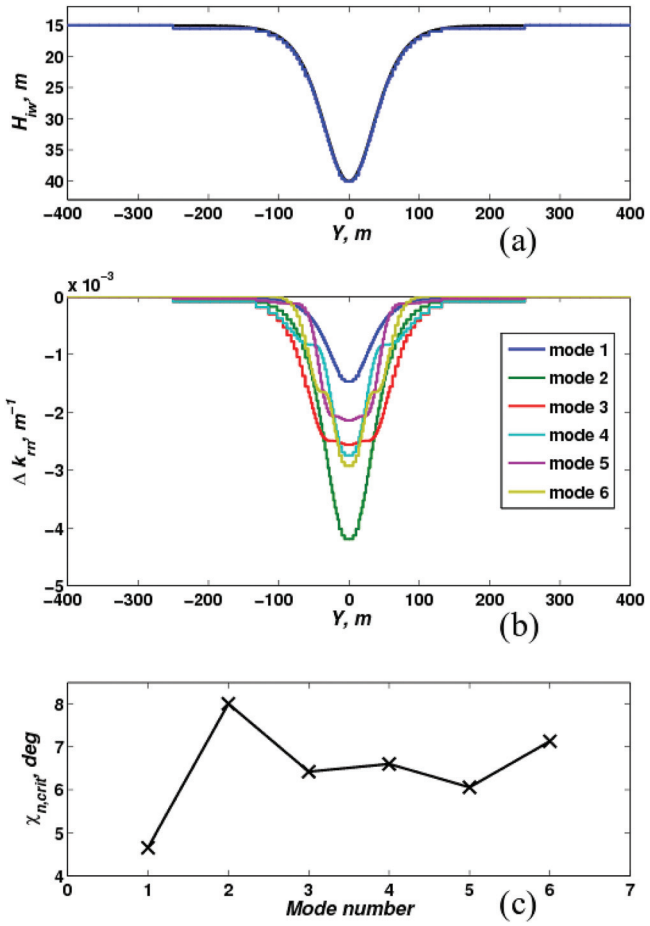

FIG. 6. (a) Internal wave of depression with amplitude of 25 m and sech^2 shape (black line). Half amplitude wave width is 130 m. The blue line represents 100 steps dividing the wave into locally range independent sectors, used in numerical modeling. (b) Changes in the horizontal modal wave numbers across the soliton internal wave with respect to the background water column values. (c) Normal mode horizontal critical angles.

white dashed line, and the horizontal location of acoustic source is shown by the red circle. By looking at the amplitude of mode one, one can clearly see the HLM pattern for $y > 0$. This is the result of interference between the direct arrival of mode 1 and its reflection from the internal wave at subcritical grazing angles. Although a single mode 1 is incident in this case, neighboring modes 2 and 3 have distinct beams of reflected energy. This phenomenon corresponds to the coupled mode reflection discussed in the previous section at grazing angles defined by Eq. (34). Amplitude plots for modes two and three transmitted through the internal wave have similar beams, but symmetrical about the internal wave. The symmetry of these beams is the result of mutual effects of mode coupling and horizontal tunneling through an internal wave.

The effect of the transparent resonance can be observed by the amplitude notch in the transmitted field of mode one [upper left pane in Fig. 7 at $(x, y) = (10\,\text{km}, -2\,\text{km})$]. It is not very distinct for this example and much stronger amplitude variations due to the transparent resonance will be shown below for the multiple wave scenario.

In Appendix B, we provide results similar to Fig. 7, but using the analytical 3D coupled mode solution [Eqs. (23) and Eq. (27)] for a single vertical interface. The reader can see how similar the acoustic fields are for the smooth shaped internal wave and its first order approximation using a single vertical interface at which a sudden depression of the thermocline occurs. A sharp interface approximating the "exact" sech^2 solution is not surprising, because the sech^2 function has a sharp slope, which the vertical sharp interface crudely mimics. The main difference in the two models is in the amplitude of the reflected acoustic intensities. While the waveguide properties change sharply for any grazing angle at the single vertical interface, the smooth shape internal wave scenario provides more gradual transition once the horizontal

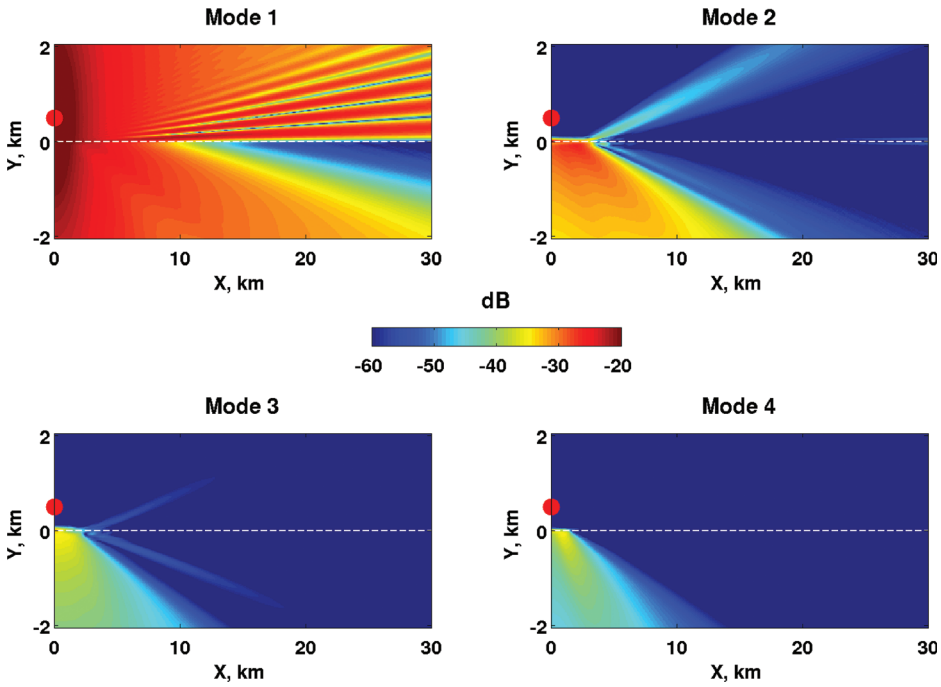

FIG. 7. Amplitudes of modes 1–4 for the case of incident mode one with unit amplitude at 1 m distance from the source and a single internal wave of 25 m amplitude centered at $y_{\text{wave}} = 0$ m. Source is located at $y_{bl} = 500$ m (red circle). White dashed line indicates the crest of internal wave.

grazing angle of the incident normal mode increases. Therefore, it is logical to expect larger amplitudes of coupled mode reflection for the single vertical interface. Note that the example shown in Appendix B is presented for the qualitative comparison only, and it is not our goal here to provide quantitative comparisons between a smooth shape internal wave and its single interface approximation (as studied for normal incidence of normal modes in Refs. 2 and 3).

B. Multiple waves

In the following example, we place two identical smooth shaped internal waves (with the same amplitude and width as in the examples above) centered at $y_{\text{wave}} = \pm 300$ m. Figure 8(a) illustrates the case of horizontal ducting with an acoustic source in between the waves ($y_s = 0$ m) and an incident mode one of unit amplitude at 1 m distance from the source. The panel depicting mode one indicates a considerable amount of energy trapped between the waves (12–15 dB difference between mode one amplitudes inside and outside of the duct). Ducted energy is known to travel over long distances, depending on the length[17] and curvature[15,16] of the natural duct, since there is (almost) no cylindrical spreading associated with its propagation. Along with the ducting of incident mode 1, one can also note ducting of a coupled mode 2, which is 15–20 dB weaker than the ducting of the initial mode 1. This effect is relatively weak, and will not likely be noticed or measured if other modes are excited at the source. Of importance is the effect of horizontal tunneling, which can be seen in the upper panel. At subcritical angles, energy from mode one leaks out of the duct and is radiated outside of the duct at the critical grazing angle. As the distance from the source increases, less energy is radiated outside of the duct; but we still note a 7 dB difference between the tunneled and ducted modal amplitudes 15 km away from the source.

We next relocate the source to $y_s = 500$ m and shift the internal wave centers to $y_{\text{wave1}} = 0$ m and $y_{\text{wave2}} = -600$ m, such that source is outside of both waves, and then repeat the simulation. The resultant modal amplitudes for the initial mode 1 are shown in Fig. 8(b). The effect of tunneled secondary ducting is clearly seen from the amplitude plot of mode 1. As discussed in Sec. IV, tunneled secondary ducting is associated with the continuous leakage of modal energy out of the duct during each interaction with the internal wave. Once mode 1 has tunneled through the first wave located at $y_{\text{wave1}} = 0$ m, part of its energy ducts in between waves (one sees increased amplitude of mode 1 in between waves at $y > 15$ km). Another part of the tunneled energy tunnels yet again with each consequent interaction with the internal waves. By comparing the upper left panel in Fig. 7 with the same panel in Fig. 8(b), one notes slight differences in the HLM patterns. This is caused by the energy of mode 1 which tunneled through the first wave ($y_{\text{wave1}} = 0$ m), was reflected by the second wave ($y_{\text{wave2}} = -600$ m), and then tunneled back through the first wave in Fig. 8(b). One may also note the secondary ducting of coupled mode 2. This effect was discussed in Sec. IV, and is a result of the

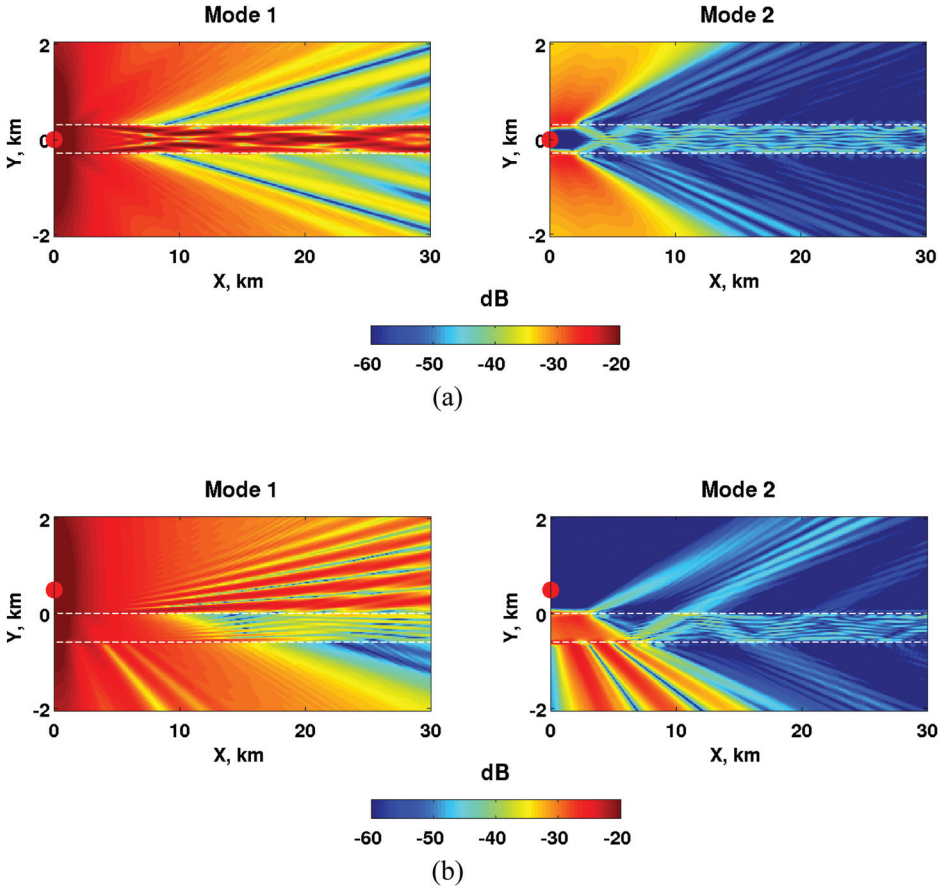

FIG. 8. (a) Horizontal ducting of normal modes. An acoustic source located at $y_s = 0$ m is in between two internal waves centered at $y_{\text{wave}} = \pm 300$ m. The incident field consists of a single mode one with unit amplitude at 1 m distance from the source. (b) Secondary ducting. An acoustic source at $(x_s, y_s) = (0,500)$ m is located just outside of the duct composed of two internal waves centered at $y_{\text{wave1}} = 0$ m and $y_{\text{wave2}} = -600$ m. The incident field consists of a single mode one of unit amplitude at 1 m distance from the source. White dashed lines indicate the crests of internal waves.

interconnection between mode coupling and horizontal tunneling. Compared to the tunneling of the initial mode 1, coupled tunneling is a less noticeable effect.

The amplitudes of the modes transmitted through both waves in Fig. 8(b) show distinct transparent resonances that are more closely spaced in grazing angle and have bigger amplitude fluctuations than for the case of one wave. We noticed in our simulations that the scintillations of the modal amplitudes transmitted through the wave train initially increase with the number of waves in the train due to cumulative transparent resonances. However, after a certain number of waves in the train (five to six in our case) having slightly different amplitudes and widths, variability in the nulls and maxima in the multiple resonances results in "smearing" of the acoustic amplitude fluctuations. This is known as saturation of the waveguide, and was observed by Fredericks *et al.*[5] in the SWARM95 experiment. He showed that for a fixed source and receiver situated across the mean direction of the internal wave crests, the root mean square of the log-intensity over a several hour time window was near 5.6 dB, the statistical value expected for fully saturated ocean waveguides.[37]

VI. CONCLUSIONS

The primary focus of this paper has been to study the physics of 3D low frequency coupled mode acoustic propagation through shallow water waveguides that contain straight internal gravity waves. This study adds value by increasing the physical understanding of the strong intensity fluctuations, which have been observed multiple times[1,4,10] for propagation across and along internal waves. The basis of our studies has been the normal mode approach, which allowed us to explain the complexities of the sound propagation in terms of simple mechanisms, mainly governed by the geometrical (modal ray path) approximation of coupled mode propagation through internal waves.

We used the simple sharp interface approximation for understanding the complicated process of continuous refraction and mode coupling. Using a single vertical interface that represented the depression of the thermocline due to an internal wave, analytical coupled mode solutions for the reflection from and transmission through such interfaces was derived. We showed that this simple approximation provided us with an analytical result that is very comparable with the precise numerical solution for sech^2 shaped internal waves. Therefore, it can be used for a wider class of ocean acoustic problems such as crossing internal waves, bottom sand waves (dunes), or even long distance surface swell.[38]

For an azimuthal analysis of the three-dimensional acoustic propagation through straight internal waves, we qualitatively divided the propagation azimuths into three sectors with respect to the horizontal grazing angles of the normal modes. Horizontal propagation of normal modes with horizontal grazing angles less than their critical values leads to an almost total reflection from the ocean internal waves. Depending on the source location relative to a group of parallel waves, this results in either the HLM effect or horizontal acoustic ducting (or anti-ducting) between the waves. In addition to primary ducting between two parallel waves, we showed that at grazing angles just below the critical values, the effects of horizontal tunneling through the waves and the following reflections from neighboring waves trap the modal energy in secondary ducts. On the other hand, at steep grazing angles (approximately 35°–90° in our examples), strong mode coupling dominates the propagation regime. The sound intensity fluctuations in these directions have been observed in a number of experiments,[1,10] and are mainly driven by strong mode coupling and its resonant-like behavior. No significant horizontal refraction is observed in this angular region. For the intermediate grazing angle range, both horizontal refraction and mode coupling were shown to be noticeable. At these angles, both mode coupled reflection from the wave fronts and secondary ducting effects are possible through mode coupling mechanisms. However, those were shown to be weak, and acoustic energy propagates mostly without horizontal trapping in this regime.

In the real ocean, internal waves, both linear and nonlinear, are not straight and have finite length. Two or more packets of nonlinear internal waves can propagate one through another and create complicated crossing structures. While the acoustic effects of curvature and termination of individual ducts on low frequency acoustics have been studied before,[15–17] the effect of internal wave crossing on acoustics has not been studied before. In our parallel studies, we are approaching this problem using the 3D parabolic equation technique.

ACKNOWLEDGMENTS

This work was supported by the Office of Naval Research under grant Nos. N00014-11-1-0195 and N00014-11-1-0701. Dr. Shmelev gratefully acknowledges the MIT/WHOI Joint Program in Oceanography for additional support.

APPENDIX A: 3D MODE COUPLING AT STRAIGHT INTERNAL WAVES

Here we describe a useful algorithm for computing three-dimensional coupled mode solutions for the acoustic pressure in waveguides with laterally varying properties along the y axis (across wave crests) and the independent of the x-coordinate (along wave crests). Assume waveguide changes to be within the segment $\lfloor y_a, y_b \rfloor$ such that

$$c(x,y,z) = \begin{cases} c^a(z), & y \le y_a, \\ c(y,z), & y_a < y < y_b, \\ c^b(z), & y \ge y_b, \end{cases} \tag{A1}$$

$$\rho(x,y,z) = \begin{cases} \rho^a(z), & y \le y_a, \\ \rho(y,z), & y_a < y < y_b, \\ \rho^b(z), & y \ge y_b. \end{cases} \tag{A2}$$

Similar to Sec. II, we apply the one-dimensional FT operator to both sides of Eq. (15), and rewrite the resultant two-dimensional separated Helmholtz equation,

$$\rho\frac{\partial}{\partial y}\left[\frac{1}{\rho}\frac{\partial\tilde{p}(k_x,y,z)}{\partial y}\right]+\rho\frac{\partial}{\partial z}\left[\frac{1}{\rho}\frac{\partial\tilde{p}(k_x,y,z)}{\partial z}\right]+\left[\frac{\omega^2}{c^2}-k_x^2\right]\tilde{p}(k_x,y,z)=-\frac{\delta(y-y_s)\delta(z-z_s)}{2\pi}. \tag{A3}$$

Our initial three-dimensional mode coupling problem is now divided into many two-dimensional problems, one for each k_x, that can be solved using known techniques. One of them is the spectral parabolic equation (PE), introduced by Orris and Collins[39] for studying three-dimensional acoustic propagation over a sloping bottom. Although the spectral PE method is robust, it has certain limitations and does not provide the explicit physics of normal mode propagation and coupling. To get the most accurate solution to our three-dimensional problem, we employ the two-way coupled mode method of solving each of the x-reduced problems.[33] Following the logic of the two-dimensional two-way mode coupling algorithm,[19,34] we divide our waveguide into $N+1$ segments by N vertical plane interfaces $y=y_j$, $j=1,\ldots,N$ such that $y_1=y_a$ and $y_N=y_b$ as shown in Fig. 9. It is further assumed that the waveguide properties do not change significantly within each segment j and are locally range independent with density and sound speed columns $\rho^j(z)$ and $c^j(z)$, respectively, and with horizontal modal wave numbers k_{rm}^j, and mode function sets $\Psi_m^j(z)$.

By placing an acoustic source into segment j_s and neglecting the contribution from the continuous part of the spectrum, the acoustic pressure field in segment j is

$$\tilde{p}^{(j)}(k_x,y,z)=\sum_{m=1}^{M}\left[\Phi_m^{(j)+}e^{ik_{ym}^j(k_x)(y-y_j)}+\Phi_m^{(j)-}e^{ik_{ym}^j(k_x)(y_j-y)}\right]\times\Psi_m^j(z)+\delta_{j,j_s}\tilde{p}^s, \tag{A4}$$

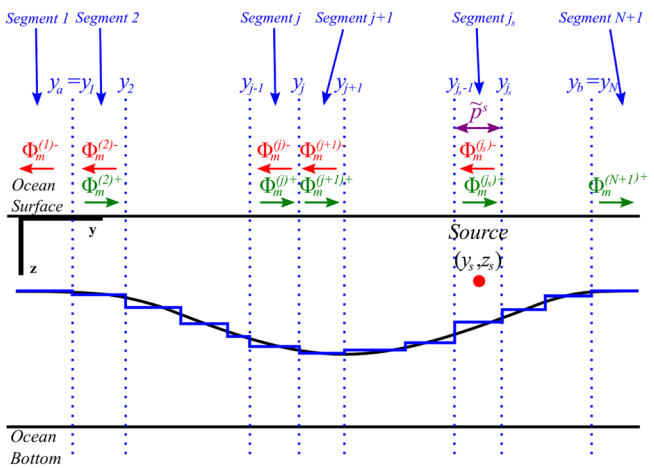

FIG. 9. (Color online) The range dependent part of the waveguide $\lfloor y_a,y_b\rfloor$ is divided by N vertical interfaces y_j, $j=1,\ldots,N$ into $N+1$ segments such that $y_1=y_a$, $y_N=y_b$. Within each segment, the waveguide properties do not change significantly and are thus locally range independent. The solution within each homogeneous segment j is a sum of right and left going plane waves with amplitudes $\Phi_m^{(j)+}$ and $\Phi_m^{(j)-}$, respectively. Segment j_s containing the acoustic source has an additional source term $\tilde{p}_s$ in the solution.

where $\Phi_m^{(j)+}$ and $\Phi_m^{(j)-}$ are the amplitudes of mode m traveling in the positive and negative directions of the y axis, respectively. By analogy with Eq. (17), the source contribution is

$$\tilde{p}^s(k_x,y,z)=\frac{i}{4\pi\rho(z_s)}\sum_{m=1}^{M}\Psi_m^{j_s}(z_s)\Psi_m^{j_s}(z)\frac{e^{ik_{ym}^{j_s}(k_x)|y-y_s|}}{k_{ym}^{j_s}(k_x)}. \tag{A5}$$

In the above, M is the number of propagating modes, and the y-component of the modal wave number in segment j is defined [similarly to Eq. (18)] as

$$k_{ym}^j(k_x)\equiv\begin{cases}\sqrt{(k_{rm}^j)^2-k_x^2}, & k_x^2\le(k_{rm}^j)^2,\\ i\sqrt{k_x^2-(k_{rm}^j)^2}, & k_x^2>(k_{rm}^j)^2.\end{cases} \tag{A6}$$

Using the matrix notation formalism of the two-dimensional version of this algorithm,[19] the appropriate boundary conditions at interface j for the acoustic pressure and the y-component of the particle velocity can be written as

$$\mathbf{\Phi}^{(j+1)+}+\mathbf{E}_2^{j+1}\mathbf{\Phi}^{(j+1)-}+\delta_{j_s,j+1}\mathbf{S}_1=\tilde{\mathbf{C}}^j(k_x)(\mathbf{E}_1^j\mathbf{\Phi}^{(j)+}+\mathbf{\Phi}^{(j)-}+\delta_{j_s,j}\mathbf{S}_2) \tag{A7}$$

and

$$\mathbf{\Phi}^{(j+1)+}-\mathbf{E}_2^{j+1}\mathbf{\Phi}^{(j+1)-}-i\delta_{j_s,j+1}\mathbf{S}_1=\hat{\mathbf{C}}^j(k_x)(\mathbf{E}_1^j\mathbf{\Phi}^{(j)+}-\mathbf{\Phi}^{(j)-}+i\delta_{j_s,j}\mathbf{S}_2), \tag{A8}$$

respectively, where $\delta_{j_s,j}$ denotes the Kronecker symbol as before. Vectors $\mathbf{\Phi}^{(j)+}$ and $\mathbf{\Phi}^{(j)-}$ consist of coefficients $\Phi_m^{(j)+}$ and $\Phi_m^{(j)-}$, respectively, the propagator matrices $\mathbf{E}_1^j$ and $\mathbf{E}_2^j$ are

$$\mathbf{E}_1^j=\mathrm{diag}(e^{ik_{ym}^j(k_x)(y_j-y_{j-1})}), \tag{A9}$$

$$\mathbf{E}_2^{j+1}=\mathrm{diag}(e^{ik_{ym}^{j+1}(k_x)(y_{j+1}-y_j)}), \tag{A10}$$

and the elements of coupling matrices $\tilde{\mathbf{C}}^j$ and $\hat{\mathbf{C}}^j$ are

$$\tilde{C}_{lm}^j(k_x)=\int\frac{\Psi_l^{j+1}(z)\Psi_m^j(z)}{\rho^{j+1}(z)}dz, \tag{A11}$$

$$\hat{C}_{lm}^j(k_x)=\frac{k_{ym}^j}{k_{yl}^{j+1}}\int\frac{\Psi_l^{j+1}(z)\Psi_m^j(z)}{\rho^j(z)}dz. \tag{A12}$$

Vectors $\mathbf{S}_1$ and $\mathbf{S}_2$ are the source contributions at the interfaces j_s-1 and j_s and consist of elements $s_{1,m}$, $m=1,\ldots,M$ and $s_{2,m}$, $m=1,\ldots,M$, respectively, where

$$s_{1,m}=\frac{i\Psi_m^{j_s}(z_s)e^{ik_{ym}^{j_s}(y_s-y_{j_s-1})}}{4\pi\rho(z_s)k_{ym}^{j_s}(k_x)},\qquad s_{2,m}=\frac{i\Psi_m^{j_s}(z_s)e^{ik_{ym}^{j_s}(y_{j_s}-y_s)}}{4\pi\rho(z_s)k_{ym}^{j_s}(k_x)}. \tag{A13}$$

The Sommerfeld radiation condition implies that

$$\mathbf{\Phi}^{(1)-}=\mathbf{0},\qquad \mathbf{\Phi}^{(N+1)+}=\mathbf{0}. \tag{A14}$$

By combining all the equations together into one matrix block form, one gets

$$\begin{bmatrix}
\mathbf{R}_2^1 & -\mathbf{I} & \mathbf{0} & & & & & & & \\
\mathbf{R}_4^1 & \mathbf{0} & -\mathbf{I} & & & & & & & \\
0 & 0 & 0 & 0 & & & & & & \\
 & & 0 & 0 & 0 & 0 & & & & \\
 & & & \mathbf{R}_1^{j_s-1} & \mathbf{R}_2^{j_s-1} & -\mathbf{I} & \mathbf{0} & & & \\
 & & & \mathbf{R}_3^{j_s-1} & \mathbf{R}_4^{j_s-1} & \mathbf{0} & -\mathbf{I} & & & \\
 & & & & & \mathbf{R}_1^{j_s} & \mathbf{R}_2^{j_s} & -\mathbf{I} & \mathbf{0} & \\
 & & & & & \mathbf{R}_3^{j_s} & \mathbf{R}_4^{j_s} & \mathbf{0} & -\mathbf{I} & \\
 & & & & & 0 & 0 & 0 & 0 & \\
 & & & & & & 0 & 0 & 0 & 0 \\
 & & & & & & & \mathbf{R}_1^N & \mathbf{R}_2^N & -\mathbf{I} \\
 & & & & & & & \mathbf{R}_3^N & \mathbf{R}_4^N & \mathbf{0}
\end{bmatrix}$$

$$\times \begin{bmatrix}
\mathbf{\Phi}^{(1)-} \\
\mathbf{\Phi}^{(2)+} \\
\mathbf{\Phi}^{(2)-} \\
\mathrm{M} \\
\mathbf{\Phi}^{(j_s-1)+} \\
\mathbf{\Phi}^{(j_s-1)-} \\
\mathbf{\Phi}^{(j_s)-} \\
\mathbf{\Phi}^{(j_s)+} \\
\mathrm{M} \\
\mathbf{\Phi}^{(N-1)+} \\
\mathbf{\Phi}^{(N-1)-} \\
\mathbf{\Phi}^{(N)+}
\end{bmatrix} = \begin{bmatrix}
\mathbf{0} \\
\mathrm{M} \\
\mathrm{M} \\
\mathbf{0} \\
\mathbf{R}_5\mathbf{S}_1 \\
\mathbf{R}_6\mathbf{S}_1 \\
\mathbf{R}_7\mathbf{S}_2 \\
\mathbf{R}_8\mathbf{S}_2 \\
\mathbf{0} \\
\mathrm{M} \\
\mathrm{M} \\
\mathbf{0}
\end{bmatrix}, \tag{A15}$$

where

$$\begin{aligned}
\mathbf{R}_1^j &= \frac{\tilde{\mathbf{C}}^j + \hat{\mathbf{C}}^j}{2}\mathbf{E}_1^j, \\
\mathbf{R}_2^j &= \frac{\tilde{\mathbf{C}}^j - \hat{\mathbf{C}}^j}{2} \\
\mathbf{R}_3^j &= \left(\mathbf{E}_2^{j+1}\right)^{-1}\frac{\tilde{\mathbf{C}}^j - \hat{\mathbf{C}}^j}{2}\mathbf{E}_1^j, \\
\mathbf{R}_4^j &= \left(\mathbf{E}_2^{j+1}\right)^{-1}\frac{\tilde{\mathbf{C}}^j + \hat{\mathbf{C}}^j}{2}, \\
\mathbf{R}_5 &= \mathbf{0}, \\
\mathbf{R}_6 &= -\left(\mathbf{E}_2^{j_s}\right)^{-1}, \\
\mathbf{R}_7 &= \frac{\tilde{\mathbf{C}}^{j_s} + \hat{\mathbf{C}}^{j_s}}{2}, \\
\mathbf{R}_8 &= \left(\mathbf{E}_2^{j_s+1}\right)^{-1}\frac{\tilde{\mathbf{C}}^{j_s} - \hat{\mathbf{C}}^{j_s}}{2},
\end{aligned} \tag{A16}$$

and $\mathbf{I}$ is the identity matrix.

Having solved the block matrix equation above for multiple evenly spaced values of k_x, the pressure kernel is constructed using Eq. (A4) and converted to $p(x, y, z)$ with the one-dimensional IFT operator [Eq. (22)].

In the absence of physical attenuation in the system (bottom loss is a good example), Eq. (A15) has a singular solution in segment j when

$$k_x = k_{rm}^j, \quad j = 1, \ldots, M.$$

Although including physical attenuation smoothes the kernel slightly, it still requires a large number of sampling points to avoid aliasing. Another method that requires much fewer sampling points consists of shifting the integration contour into the complex plane by an offset ε. This technique is described in details in Refs. 18 and 19. In our applications, we evaluated the kernel at $N_{k_x} = 2^{13}$ points, and the value of the offset that guaranteed the wrap-around attenuation to be down by 50 dB was

$$\varepsilon = \frac{12k_x^{\max}}{2\pi(N_{k_x} - 1)\log e}, \tag{A17}$$

which is four times greater than that required for applications of sound reflection from the sea bottom.[19]

APPENDIX B: HORIZONTAL LLOYD'S MIRROR AT A SINGLE VERTICAL INTERFACE

We provide an illustrative example of an analytical solution for 3D coupled mode reflection and transmission through a vertical interface using Eqs. (23) and (27) in Figs. 10 and 11. The background waveguide model (region 0) is identical to that used in Sec. V, and its perturbation in region 1 is modeled by a sudden depression of the thermocline by $\Delta H_{iw} = 25$ m along the y axis (Fig. 10). Similar to the smoothed internal wave numerical example shown in Fig. 7, we set the incident acoustic field to be a single mode one with unit amplitude at 1 m horizontal distance from the source location. Figure 11 shows the resultant amplitudes of modes 1–4. The reader will notice strong similarities between the acoustic fields for a smooth shaped internal wave in Fig. 7 and its single vertical interface approximation.

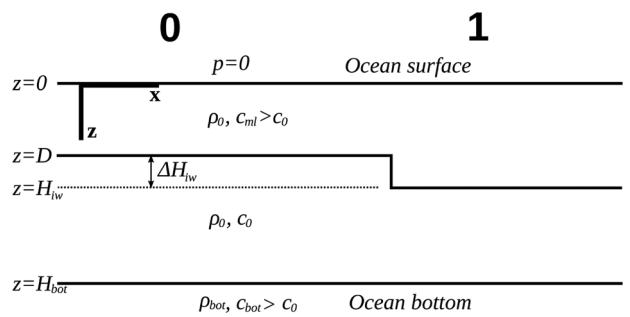

FIG. 10. A sharp vertical interface divides a waveguide into an unperturbed part (region 0) and a perturbed part (region 1). The waveguide consists of two homogeneous water layers (the upper layer having slightly higher temperature and sound speed) overlaying a bottom fluid half space. Perturbation of the water column in region 1 is modeled by depression of the interface between the water layers by ΔH_{iw}.

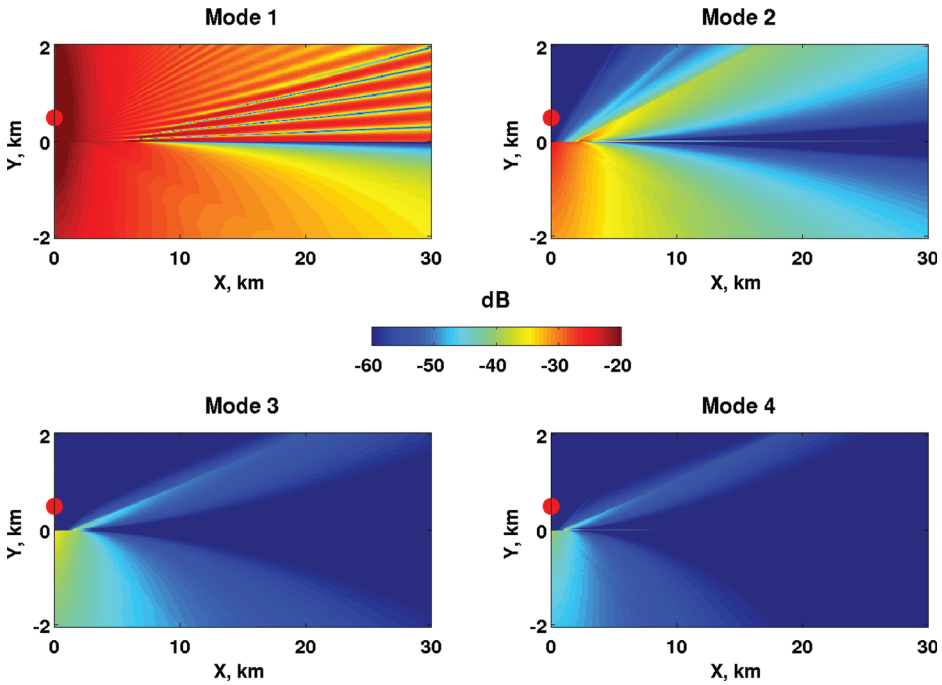

FIG. 11. Amplitudes of modes 1–4 for the case of mode one incident from a source located at $(x_s, y_s) = (0, 500)$ m. The vertical interface along $y = 0$ represents a sudden thermocline depression of 25 m amplitude.

[1]J. Zhou, Z. Zhang, and P. H. Rogers, "Resonant interaction of sound wave with internal solitons in the coastal zone," J. Acoust. Soc. Am. **90**, 2042–2054 (1991).

[2]J. C. Preisig and T. F. Duda, "Coupled acoustic mode propagation through continental-shelf internal solitary waves," IEEE J. Ocean. Eng. **22**, 256–269 (1997).

[3]T. F. Duda and J. C. Preisig, "A modeling study of acoustic propagation through moving shallow-water solitary wave packets," IEEE J. Ocean. Eng. **24**, 16–32 (1999).

[4]J. R. Apel, M. Badiey, C. S. Chiu, S. Finette, R. Headrick, J. Kemp, J. F. Lynch, A. Newhall, M. H. Orr, B. H. Pasewark, D. Tielbuerger, A. Turgut, K. Heidt, and S. Volf, "An overview of the 1995 SWARM shallow-water internal wave acoustic scattering experiment," IEEE J. Ocean. Eng. **22**, 465–500 (1997).

[5]A. Fredericks, J. A. Colosi, J. F. Lynch, and G. Gawarkiewicz, "Analysis of multipath scintillations from long range acoustic transmissions on the New England continental slope and shelf," J. Acoust. Soc. Am. **117**, 1038–1057 (2005).

[6]M. Badiey, J. Lynch, X. Tang, and J. Apel, "Azimuthal and temporal dependence of sound propagation due to shallow water internal waves," IEEE J. Ocean. Eng. **27**, 117–129 (2002).

[7]B. G. Katsnelson and S. A. Pereselkov, "Low-frequency horizontal acoustic refraction caused by internal wave solitons in a shallow sea," Acoust. Phys. **46**, 684–691 (2000).

[8]R. Oba and S. Finette, "Acoustic propagation through anisotropic wave fields: transmission loss, cross range coherence, and horizontal refraction," J. Acoust. Soc. Am. **111**, 769–784 (2002).

[9]R. Oba and S. Finette, "Horizontal array beamforming in an azimuthally anisotropic internal wave field," J. Acoust. Soc. Am. **114**, 131–144 (2003).

[10]D. J. Tang, J. N. Moum, J. F. Lynch, P. Abbot, R. Chapmann, P. H. Dahl, T. F. Duda, G. Gawarkiewicz, S. Glenn, J. A. Goff, H. Graber, J. Kemp, A. Maffei, J. D. Nash, and A. Newhall, "Shallow Water'06, A joint acoustic propagation/nonlinear internal wave physics experiment," Oceanogr. **20**, 156–167 (2007).

[11]T. F. Duda, J. M. Collis, Y.-T. Lin, A. E. Newhall, J. F. Lynch, and H. A. DeFerrari, "Horizontal coherence of low-frequency fixed-path sound in a continental shelf region with internal-wave activity," J. Acoust. Soc. Am. **131**, 1782–1797 (2012).

[12]A. A. Shmelev, "Three-dimensional acoustic propagation through shallow water internal, surface gravity and bottom sediment waves," Ph.D. thesis, MIT/WHOI Joint Program in Oceanography (2011).

[13]M. Badiey, B. G. Katsnelson, Y.-T. Lin, and J. F. Lynch, "Observation of acoustic multipath arrivals in the horizontal plane due to approaching nonlinear internal waves," J. Acoust. Soc. Am. **129**, EL141–EL147 (2011).

[14]J. F. Lynch, C. Emerson, P. A. Abbot, G. G. Gawarkiewitz, A. E. Newhall, Y.-T. Lin, and T. F. Duda, "On whether azimuthal isotropy and alongshelf translational invariance are present in low-frequency acoustic propagation along the New-Jersey shelfbreak," J. Acoust. Soc. Am. **131**, 1762–1781 (2012).

[15]J. F. Lynch, Y.-T. Lin, T. F. Duda, and A. E. Newhall, "Acoustic ducting, reflection, refraction, and dispersion by curved nonlinear internal waves in shallow water," IEEE J. Ocean. Eng. **35**, 12–27 (2010).

[16]Y.-T. Lin, K. G. McMahon, J. F. Lynch, and W. L. Siegmann, "Horizontal ducting of sound by curved nonlinear internal gravity waves in the continental shelf areas," J. Acoust. Soc. Am. **133**, 37–49 (2013).

[17]Y.-T. Lin, T. F. Duda, and J. F. Lynch, "Acoustic mode radiation from the termination of a truncated nonlinear internal gravity wave duct in a shallow ocean area," J. Acoust. Soc. Am. **126**, 1752–1765 (2009).

[18]H. Schmidt, "SAFARI: Seismo-acoustic fast field algorithm for range independent environments, User's Guide," SACLANT Report No. SR-113, SACLANT Undersea Research Centre, La Spezia, Italy (1988).

[19]F. B. Jensen, W. A. Kuperman, M. B. Porter, and H. Schmidt, *Computational Ocean Acoustics* (Springer-Verlag, New York, 1993), p. 783.

[20]M. Badiey and B. G. Katsnelson, "Frequency dependence and intensity fluctuations due to shallow water internal waves," J. Acoust. Soc. Am. **122**, 747–760 (2007).

[21]C. J. Higham and C. T. Tindle, "Coupled perturbed modes and internal solitary waves," J. Acoust. Soc. Am. **113**, 2515–2522 (2003).

[22]E. K. Westwood, C. T. Tindle, and N. R. Chapman, "A normal mode model for acousto-elastic ocean environments," J. Acoust. Soc. Am. **100**, 3631–3645 (1996).

[23]K. G. McMahon, L. K. Reilly-Raska, J. F. Lynch, T. F. Duda, and W. L. Siegmann, "Horizontal Lloyd mirror patterns from straight and curved nonlinear internal waves," J. Acoust. Soc. Am. **131**, 1689–1700 (2012).

[24]J. F. Lynch, J. A. Colosi, G. G. Gawarkiewicz, T. F. Duda, A. D. Pierce, M. Badiey, B. G. Katsnelson, J. E. Miller, W. Siegmann, C.-S. Chiu, and A. Newhall, "Consideration of fine-scale coastal oceanography and 3-D acoustic effects for the ESME sound exposure model," IEEE J. Ocean. Eng. **31**, 33–48 (2006).

[25]P. G. Frank, P. G. Bergmann, and A. Yaspan, "Ray acoustics," in *Physics of Sound in the Sea* (Peninsula Publishing, Los Altos, CA, 1989), pp. 41–69.

[26]W. M. Carey, "Lloyd's mirror-image interference effects," Acoust. Today. **5**, 14–20 (2009).

[27]E. Merzbacher, *Quantum Mechanics*, 2nd ed. (Wiley, New York, 1970), Chap. 4.4.

[28]P. M. Morse and H. Fechbach, *Methods of Theoretical Physics* (McGraw-Hill, New York, 1953), pp. 1099–1100.
[29]F. B. Jensen and H. Schmidt, "Subcritical penetration of narrow Gaussian beams into sediments," J. Acoust. Soc. Am. **82**, 574–579 (1987).
[30]Y.-T. Lin, T. F. Duda, and A. E. Newhall, "Three-dimensional sound propagation models using the parabolic equation approximation and the split-step Fourier method," J. Comput. Acoust. **21**, 1250018 (2013).
[31]R. Cheng, P. J. Morris, and K. S. Brentner, "A three dimensional parabolic equation method for sound propagation in moving inhomogeneous media," J. Acoust. Soc. Am. **126**, 1700–1710 (2009).
[32]S. R. Rutherford, "An examination of mode coupled theory as applied to underwater sound propagation," technical report No. ARL-TR-79-44, Applied Research Laboratories, Austin, TX (1979).
[33]J. A. Fawcett and T. W. Dawson, "Fourier synthesis of three-dimensional scattering in a two-dimensional oceanic waveguide using boundary integral equation methods," J. Acoust. Soc. Am. **88**, 1913–1920 (1990).
[34]R. B. Evans, "A coupled mode solution for acoustic propagation in a waveguide with stepwise depth variations of a penetrable bottom," J. Acoust. Soc. Am. **74**, 188–195 (1983).
[35]D. J. Korteweg and G. de Vries, "On the change of form of long waves advancing in a rectangular canal, and on a new type of long stationary waves," Philos. Mag. **39**, 422–443 (1895).
[36]M. B. Porter, "The KRAKEN normal mode program," SACLANTTECN Memorandum No. SM-245, SACLANT Undersea Research Centre, La Spezia, Italy (1991).
[37]I. Dyer, "Statistics of sound propagation in the ocean," J. Acoust. Soc. Am. **48**, 337–345 (1970).
[38]A. A. Shmelev, J. F. Lynch, Y.-T. Lin, A. E. Newhall, and T. F. Duda, "Range dependent acoustic intensity scintillations due to focusing, defocusing, and scattering by sea swell and bottom sediment waves (A)," J. Acoust. Soc. Am. **132**, 1944 (2012).
[39]G. J. Orris and M. D. Collins, "The spectral parabolic equation and three-dimensional backscattering," J. Acoust. Soc. Am. **96**, 1725–1731 (1994).